Solar Energy 159 (2018) 283–290

Contents lists available at ScienceDirect

Solar Energy

journal homepage: www.elsevier.com/locate/solener

Density functional theory study on ruthenium dyes and dye@TiO_2 assemblies for dye sensitized solar cell applications

Ramesh Kumar Chitumalla, Joonkyung Jang*

Department of Nanoenergy Engineering, Pusan National University, Busan 609-735, Republic of Korea

ARTICLE INFO

Keywords:
Cyclometalation
Density functional theory
Dye sensitized solar cell
Ru-sensitizers
Solvent effect
Thiocyanate-free

ABSTRACT

Cyclometalated ruthenium dyes improve significantly the performance of dye sensitized solar cells (DSSCs) based on conventional ruthenium dyes. Here, this study examined four thiocyanate-free cyclometalated ruthenium dyes using the density functional theory (DFT). The geometrical, electronic structural, and photophysical propertiesof the dyes and the dyes tethered to a TiO_2 surface were examined in both the presence and absence of an acetonitrile solvent. The Kohn-Sham eigenvalues of the molecular orbitals of the dyes were destabilized by *ca.* 2 eV in the presence of the solvent. The absorption peaks did not change significantly in position but hyperchromic shifts of more than two-fold occurred. When adsorbed on a TiO_2 surface, the dyes showed redshifted absorption of approximately 20 nm. To the best of our knowledge, a systematic and comprehensive first-principles investigation on cyclometalated ruthenium dyes in vacuum, solvent, and tethered to TiO_2 has been carried out for the first time.

1. Introduction

Dye sensitized solar cells (DSSC) have attracted considerable interest because of their efficient light conversion and high performance at low cost (O'Regan and Grätzel, 1991). In DSSCs, ruthenium complexes equipped with polypyridyl ligands have been proposed as alternative sensitizers owing to their ultimate photophysical and photochemical properties (Ardo and Meyer, 2009). The best (efficiency *ca.* 13%) metal organic ruthenium complexes employed in DSSCs (**N3**, **N719,** and **N749**) are equipped with thiocyanate (NCS) ligands. On the other hand, they can be separated easily from the ruthenium center owing to the labile nature of NCS ligands upon thermal stress or light soaking, which makes the DSSC device unstable (Tuyet Nguyen et al., 2010). Another disadvantage of conventional ruthenium polypyridyl sensitizers is the relatively poor capability of their near-infrared (NIR) spectral absorption (Nazeeruddin et al., 2001). To enhance the power conversion efficiency, NIR light absorbing dyes are essential because approximately 50% of the sunlight falls in the NIR spectral region (700 nm–1 mm) (Singh and Sharma, 2014). Thiocyanate-free cyclometalated ruthenium dyes can improve the stability of DSSCs significantly (Bessho et al., 2009) and also they are NIR sensitizers (Wadman et al., 2007).

The electrolyte, which is commonly comprised of additives dissolved in an organic solvent, serves as a redox shuttle and as a fundamental component of DSSCs. Because the solvent in the electrolyte plays a significant role and strongly affects the device stability and efficiency, many polar organic solvents have been proposed to enhance the efficiency of a DSSC. In addition, the influence on the stability and efficiency of the device, the solvent also plays the significant role in the kinetics of the dye@TiO_2 interface. Acetonitrile is one of the best and widely used electrolyte solvents in DSSCs because of its low viscosity and excellent solubility. Nevertheless, acetonitrile has a low boiling point (82 °C); it has been used as the main solvent in DSSCs with the highest solar to power conversion efficiency (13%) (Mathew et al., 2014). The dye interactions with the solvent molecules causes significant variations in their physical and chemical properties (Szafran et al., 1993). Therefore, it is imperative to include the solvation effects for the correct description of the experimental excitation spectrum of ruthenium complexes in theoretical calculations. Filippo and others reported the influence of various solvents on the electrochemical and optical properties of popular ruthenium polypyridyl complexes (Fantacci et al., 2004; Xu et al., 2006; Byrne et al., 2016) and observed significant destabilization (up to 4 eV) of the molecular orbitals upon solvation.

Despite several reports on the solvent effect on either isolated ruthenium dyes or dye@TiO_2 assemblies, a comprehensive theoretical investigation on cyclometalated ruthenium dyes in vacuum, solvent, and tethered to TiO_2 have not been addressed systematically to the best of our knowledge. This study examined four ruthenium sensitizers, either isolated or adsorbed on a titanium oxide surface, using density

* Corresponding author.
E-mail address: jkjang@pusan.ac.kr (J. Jang).

https://doi.org/10.1016/j.solener.2017.10.058
Received 16 May 2017; Received in revised form 29 August 2017; Accepted 20 October 2017
Available online 09 November 2017
0038-092X/

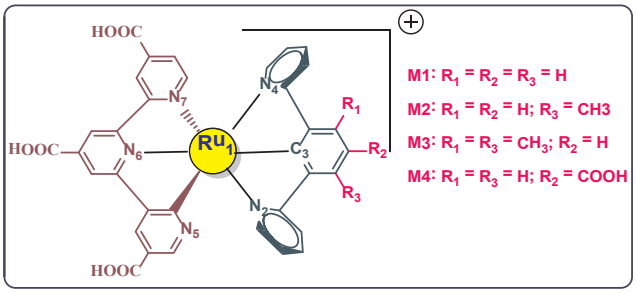

Fig. 1. Molecular geometries of the four cyclometalated ruthenium complexes considered in this study.

functional theory (DFT). The studied dyes differ in the substitution on the ancillary ligand. For the substitutions, we have opted one methyl (**M2**), two methyls (**M3**), and carboxylic (**M4**) groups to explore their electron donating/withdrawing nature on the electrochemical and optical properties. The introduction of methyl and the carboxylic groups is expected to enhance the optical absorption and the dye anchoring, respectively. The four ruthenium sensitizers (**M1**-**M4**, see Fig. 1) with or without the acetonitrile solvent were studied. The acetonitrile solvent was modeled using the self-consistent reaction field (SCRF) model (Tapia and Goscinski, 1975), which is used extensively on both the semiempirical (Karelson and Zerner, 1992) and *ab initio* molecular orbital (MO) theory (Wong et al., 1992). The effects of the solvent on geometrical, electronic, and photophysical properties of the isolated dyes and dyes tethered to a TiO_2 surface were also examined.

2. Computational details

The geometries of the sensitizers in their ground states (S_0) were optimized in the gas phase and re-optimized in acetonitrile using the B3LYP (Becke, 1993; Lee et al., 1988) functional. TDDFT calculations were performed to obtain the UV-visible absorption spectra of the optimized structures. The 6–31g(d,p) basis set and the Los Alamos effective core potential (Lanl2DZ) (Hay and Wadt, 1985) were used for the lighter (H, C, N, and O) and heavier elements (Ru), respectively. The effective core potential replaces the core electrons of Ru, but the outer core ($4s^2 4p^6$) and $4d^6$ valence electrons are considered explicitly. The solvent environment was modeled using the integral equation formalism PCM within the SCRF theory. With the exception of the optimization of dye@TiO_2 assemblies, all the DFT and TDDFT simulations were performed using the Gaussian09 suite (Frisch et al., 2013). All the UV-visible absorption spectra were broadened with the Gaussian line shapes with a full-width at half-maximum of 2000 cm^{-1}. The first 25 singlet-singlet allowed transitions were calculated to obtain the smooth part of the optical absorption spectra in the TDDFT simulations.

The interfacial electron transfer process between the anode (titanium dioxide) and dye-sensitizer has attracted considerable interest recently (Liu et al., 2012; Pastore et al., 2016). To elucidate the adsorption behavior and binding modes of the dyes on TiO_2, the periodic plane-wave DFT simulations were performed using the VASP 5.4 program (Kresse and Hafner, 1993; Kresse and Furthmüller, 1996). The stoichiometric structure of the TiO_2 cluster was taken to be a TiO_2 semiconductor, an anatase (1 0 1) slab reported by Lundqvist et al. (2006). We have considered this TiO_2 cluster over TiO_2 slab for computational advantage. The $(TiO_2)_{38}$ cluster is regarded as an isolated molecule and was optimized using the generalized gradient-corrected approximation (GGA) method. The PBE (Perdew et al., 1996) functional was employed for the exchange-correlation in combination with the plane waves and projector augmented wave methods (Blöchl, 1994; Kresse and Joubert, 1999). The plane waves were cutoff at a 400 eV kinetic energy. The Brillouin zone was sampled using the gamma-centered K-points of 1 × 1 × 1 when optimizing the geometries of the dye@TiO_2 assemblies. Geometry optimization was taken to be complete when the residual forces were less than 1 meV/Å. A large cubic supercell (a = b = c = 25 Å) was chosen to avoid the spurious interactions of the system with its images in all three directions. First, the bare $(TiO_2)_{38}$ cluster and each dye were optimized, followed by optimization of the dye@TiO_2 assembly. As the dyes have a unit positive charge, a background charge was introduced in the supercell to maintain the electrical neutrality of the periodic system. The spurious electrostatic interactions between the adjacent supercells were corrected as a result of the introduced background charge by imposing monopole and multipole terms, as implemented in VASP (Neugebauer and Scheffler, 1992; Makov and Payne, 1995).

The semilocal PBE functional of GGA (employed in VASP) tends to underestimate the semiconductor band gap (Di Valentin et al., 2006). Therefore, in the TDDFT simulations (in *G09*) of the dye@TiO_2 assemblies, hybrid B3LYP exchange-correlation functional was used, in which a part of the exact Hartree-Fock exchange is considered along with the DFT exchange. For computational simplicity, a relatively small basis set, 3-21G(d), was used for the dye@TiO_2 assemblies, which was used extensively for the simulation of such a large system (De Angelis et al., 2004, 2007a,b).

3. Results and discussion

3.1. Isolated ruthenium sensitizers

3.1.1. Ground state geometries of the isolated ruthenium sensitizers

The optimized geometries of the sensitizers with the lowest energies are illustrated in the Supplementary Information (Fig. S1). Table S1 (Supplementary Information) lists the important geometrical parameters around the ruthenium center of the four sensitizers obtained in the acetonitrile solvent and in vacuum. When immersed in an acetonitrile solvent, the Ru—C bond distance decreased by 0.001 Å for **M1** to **M3**, and by 0.005 Å for **M4**. In most cases, the reported bond lengths decreased by only 0.001 Å in the presence of an acetonitrile solvent. The Ru—C bond is the shortest among the reported bond lengths for all the dyes. The Ru—C bond was elongated by 0.008 Å for **M3** when two electron donating groups (—CH_3) were present, whereas the same bond was shortened by 0.012 Å for **M4** due to the electron withdrawing group (—COOH). The table also shows that the Ru—N bond trans to the cyclometalated bond is shorter than those of the other Ru—N bonds. All the bond angles reported varied from 77.4° to 78.5°. The bond angles changed either by 0.1° or remained unaltered upon solvation. Therefore, the influence of an acetonitrile solvent on the geometrical parameters is only minor.

3.1.2. Electronic structure, frontier molecular orbitals, and HOMO–LUMO gaps of the dyes

Fig. 2 shows a schematic diagram of the comparative electronic structures of the isolated sensitizers in a vacuum and in acetonitrile. In the figure, the energies of the frontier orbitals in vacuum and in acetonitrile were plotted according to their energies. The HOMO-LUMO gaps (HLG) are shown with solid arrows, and the upshifts (destabilization of MOs) of the energies are represented by dotted arrows. As shown in the figure, all the reported MO energy levels were upshifted by *ca.* 2 eV upon solvation. As the HOMO and LUMO values are crucial measures of dye regeneration and electron injection in DSSCs, this study discusses the solvent effects on those values in detail. The HOMO energies in the solvent are −5.51, −5.42, −5.45, and −5.70 eV, which are destabilized by *ca.* 2.2 eV relative to those obtained in a vacuum viz., −7.72, −7.60, −7.62, and −7.89 eV for **M1**, **M2**, **M3**, and **M4**, respectively. Similarly, the LUMO energies of the dyes are destabilized by *ca.* 2.2 eV with switching from the vacuum (−5.21, −5.18, −5.16, and −5.31) to the solvent (−2.99, −2.98, −2.99, and −3.05 eV). The destabilization of the orbital energies reflects the stabilization of the positively charged metal center (Ru^{2+}) in acetonitrile (Fantacci et al., 2004). Despite the large destabilization in the HOMO

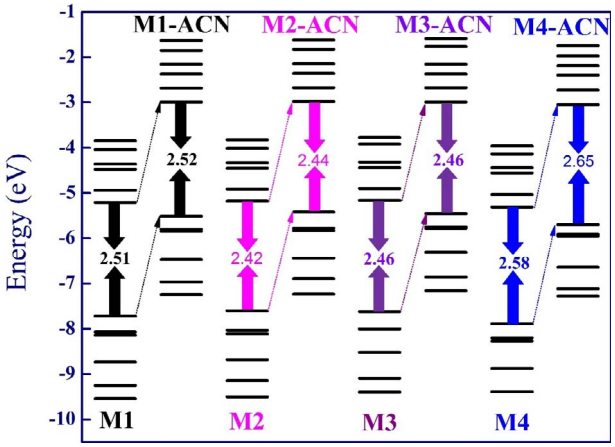

Fig. 2. Comparison of the energy levels of the sensitizers **M1**-**M4** in vacuum and in acetonitrile (ACN). The solid arrows represent the HOMO-LUMO gaps and dotted arrows represent the destabilization due to solvation.

and LUMO energies of the sensitizers, the HLG values did not change much upon solvation. The maximum change in HLG with solvation was observed for **M4** (0.07 eV).

For the effective injection of electrons, the LUMO energy of a sensitizer must be above the conduction band (−4.2 eV) of the photoanode. The LUMO energies obtained in the solvent are above and energetically close to the TiO_2 conduction band, so that electrons could be injected easily. In contrast, the LUMO energies in the vacuum are below the conduction band of the anode. The redox potentials (−HOMO) of all the sensitizers obtained in the solvent are below and close to the redox potential (−5.20 eV) of the redox couple (I^-/I_3^-), so regeneration of the dyes can be facilitated. The HOMO and LUMO energies of the sensitizers in the solvent are suitable for DSSC applications. This shows that the presence of a solvent is essential for a correct description of their electrochemical behavior in theoretical simulations.

Fig. 3 presents the isodensity plots (isovalue ± 0.02e/a.u^3) of the frontier molecular orbitals (FMOs) of the sensitizers with and without the solvent. The present ruthenium sensitizers can be divided into three parts, i.e., ruthenium, TPY (anchoring) ligand, and TPY-C (cyclometalated or ancillary) ligand. For all sensitizers, the electron density for HOMO is populated mainly over ruthenium and the TPY-C ligand. In

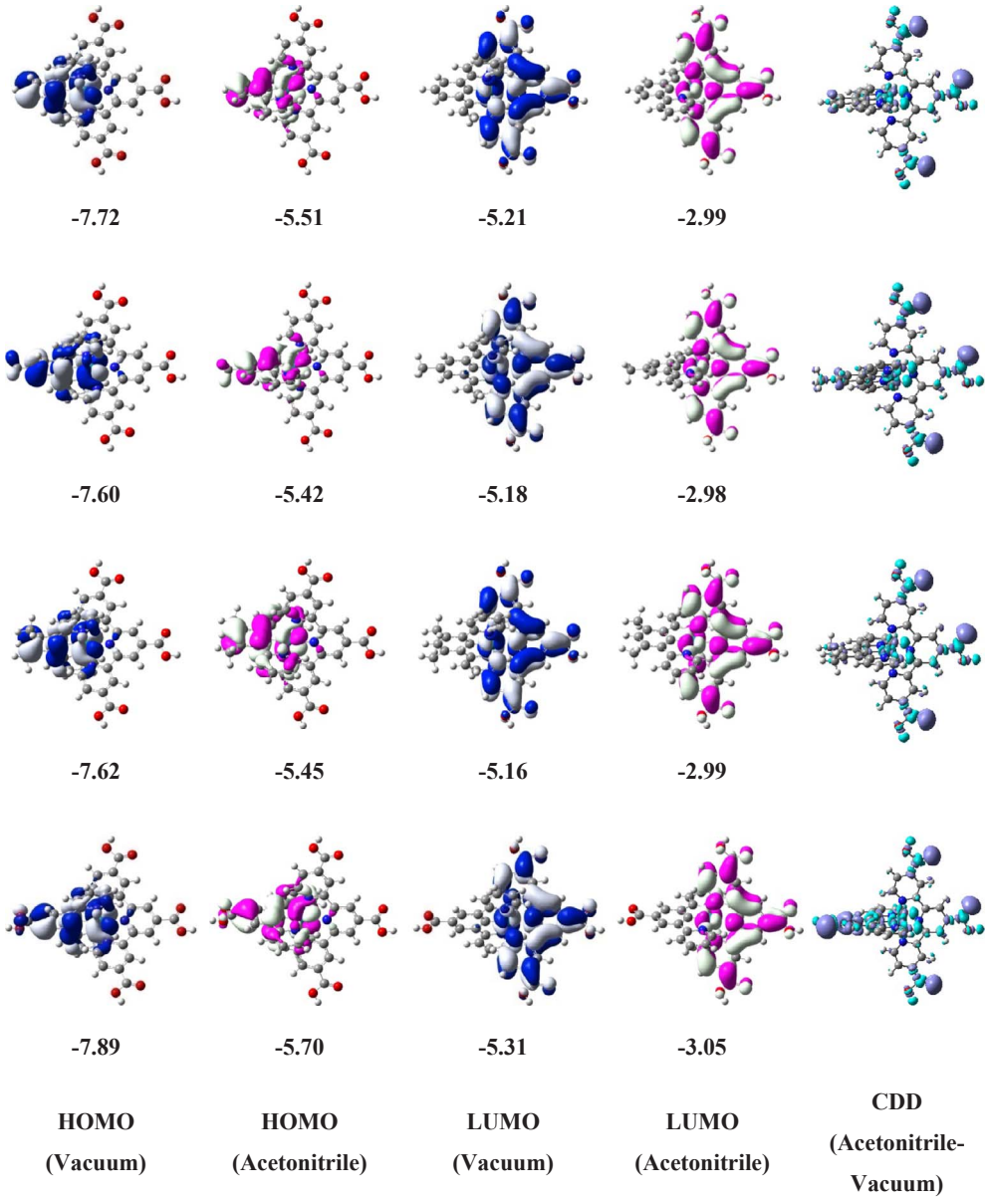

Fig. 3. Frontier molecular orbitals of the dyes **M1** (first row) – **M4** (last row) in acetonitrile and in vacuum. The charge density difference plots of the dyes from the solvent to vacuum are also shown in the last column.

Table 1
Partial molecular orbital composition (%) of the sensitizers in acetonitrile and in a vacuum (parenthesized).

MO	Ru	TPY (Anchoring)	TPY-C (Ancillary)	Ru	TPY (Anchoring)	TPY-C (Ancillary)
	M1			**M2**		
L+4	1.6 (2.2)	0.5 (0.4)	97.9 (97.4)	1.5 (2.2)	0.5 (0.4)	98.0 (97.5)
L+3	1.1 (1.8)	96.9 (96.0)	2.0 (2.2)	1.1 (1.8)	96.9 (96.0)	1.9 (2.2)
L+2	1.0 (1.2)	98.9 (97.8)	0.1 (1.0)	1.0 (1.3)	98.9 (97.7)	0.1 (1.0)
L+1	4.1 (4.6)	95.2 (94.9)	0.6 (0.5)	4.2 (4.6)	95.2 (94.9)	0.6 (0.5)
L+0	11.7 (13.7)	86.1 (81.6)	2.1 (4.7)	11.9 (13.9)	85.9 (81.3)	2.2 (4.8)
H-0	49.8 (53.9)	5.3 (9.3)	44.9 (36.8)	46.2 (49.9)	4.9 (8.9)	48.8 (41.2)
H-1	69.3 (70.8)	21.7 (18.3)	9.0 (10.9)	69.0 (70.5)	22.0 (18.6)	9.1 (10.9)
H-2	65.4 (69.3)	13.8 (11.7)	20.8 (19.1)	64.9 (68.8)	13.8 (11.7)	21.3 (19.5)
H-3	6.7 (11.9)	2.3 (3.1)	91.0 (85.0)	7.2 (12.6)	2.4 (3.2)	90.3 (84.2)
H-4	25.8 (33.7)	5.3 (9.1)	68.8 (57.2)	30.5 (39.0)	5.8 (9.6)	63.7 (51.4)
	M3			**M4**		
L+4	2.2 (2.9)	0.2 (0.3)	97.6 (96.8)	1.4 (2.1)	1.0 (0.4)	97.6 (97.6)
L+3	1.0 (1.7)	97.0 (96.0)	2.0 (2.3)	1.2 (1.9)	96.4 (96.1)	2.4 (2.1)
L+2	1.0 (1.3)	98.9 (97.6)	0.1 (1.1)	0.8 (1.2)	99.1 (97.8)	0.1 (1.0)
L+1	4.2 (4.7)	95.1 (94.8)	0.7 (0.5)	3.9 (4.4)	95.5 (95.2)	0.6 (0.4)
L+0	12.0 (14.0)	85.8 (81.0)	2.2 (4.9)	10.9 (13.3)	87.1 (82.0)	2.0 (4.7)
H-0	47.6 (51.6)	5.1 (9.0)	47.3 (39.4)	51.3 (53.3)	5.4 (9.0)	43.2 (37.7)
H-1	68.9 (69.8)	22.0 (18.2)	9.2 (12.0)	70.0 (71.3)	20.7 (17.8)	9.2 (10.9)
H-2	59.1 (62.5)	12.2 (10.5)	28.7 (27.0)	67.4 (69.7)	14.2 (11.5)	18.4 (18.8)
H-3	12.1 (20.2)	3.6 (4.6)	84.3 (75.2)	4.8 (11.5)	1.9 (2.9)	93.4 (85.6)
H-4	29.1 (37.3)	5.5 (9.2)	65.4 (53.5)	22.3 (34.5)	5.0 (9.4)	72.7 (56.1)

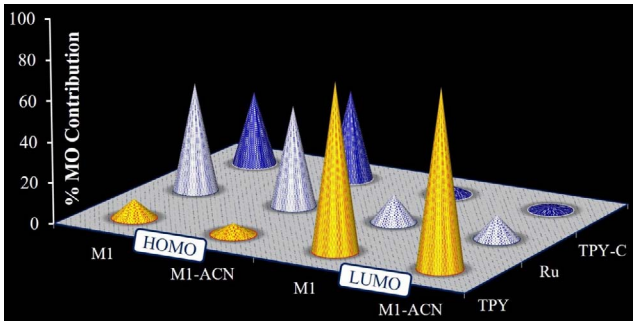

Fig. 4. Partial molecular orbital contribution of TPY, ruthenium, and TPY-C in HOMO and LUMO of the dye **M1** in vacuum and in acetonitrile (ACN).

contrast, the electron densities of LUMOs are transferred to the anchoring TPY ligands. The electron density distribution pattern obtained in the solvent does not differ significantly from that in a vacuum. Partial MO composition analysis was carried out on five occupied and five unoccupied MOs with respect to the three parts (*vide supra*). Except for the LUMO+4, in all unoccupied molecular orbitals reported in Table 1, the electron density is mostly populated over the anchoring TPY ligand, which facilitates electron injection. The electron density in the occupied orbitals is delocalized on the ruthenium center and on the ancillary TPY-C ligand. The robust charge transfer from the HOMO to LUMO confirms the transition due to intramolecular charge transfer in their absorption spectra.

The electron density dispersion in various molecular orbitals of the dyes was studied quantitatively by the partial molecular orbitals composition given in Table 1. The table shows that the electron density on the ruthenium center decreases by introducing the solvent. In addition, the electron density is increased on the anchoring (TPY) ligand (except few occupied orbitals). On the other hand, the electron density on the ancillary ligand is not affected uniformly by the solvent; the electron density increased for few molecular orbitals but decreased for the other orbitals. Interestingly, the solvation effects on the electron density distribution were similar for all the dyes investigated. Fig. 3 also presents the charge density difference plots of the dyes in a solvent in comparison to that in a vacuum. A high charge density difference was observed only at -COOH groups. The purple and blue colors represent the charge accumulation and depletion, respectively. Fig. 4 shows the influence of solvation on the molecular orbital (HOMO and LUMO of **M1**) composition projected onto the TPY, Ru, and TPY-C. Fig. S2 in the Supplementary Information presents the corresponding figures of **M2** to **M4**. Although solvation affects the composition of the FMOs moderately, their energies were intensely affected.

Natural population analysis for the ground (S_0) and the first singlet excited state (S_1) of the sensitizers was carried out to estimate the charge transferred from the ancillary ligand to the anchoring ligand. Table 2 lists the results obtained in acetonitrile were compared with those of a vacuum. All the investigated sensitizers have a unit positive charge. The decrease in the charge of TPY (increase for TPY-C) from the ground to the excited state indicates the shift of the electron density from TPY-C to TPY upon excitation.

3.1.3. Photophysical properties of four sensitizers in solvent and vacuum

Fig. 5 presents the simulated optical absorption spectra of the sensitizers in the solvent and vacuum. The spectra do not significantly vary

Table 2
Charge distribution (in e) from the natural population analysis for the sensitizers **M1**-**M4** in the S_0 and S_1 states at the B3LYP/6-31G(d,p) and TDB3LYP/6-31G(d,p) levels of theory, respectively.

Dye	q(S_0)			q(S_1)			Δq[a]		
	Ru	TPY	TPY-C	Ru	TPY	TPY-C	Ru	TPY	TPY-C
M1	0.140 (0.136)	0.582 (0.574)	0.277 (0.290)	0.320 (0.296)	0.072 (0.131)	0.607 (0.573)	0.180 (0.160)	−0.510 (−0.443)	0.330 (0.283)
M2	0.141 (0.138)	0.575 (0.566)	0.283 (0.296)	0.583 (0.282)	−0.226 (0.118)	0.643 (0.600)	0.442 (0.144)	−0.801 (−0.448)	0.360 (0.304)
M3	0.135 (0.132)	0.575 (0.565)	0.290 (0.303)	0.306 (0.567)	0.065 (−0.232)	0.629 (0.664)	0.171 (0.435)	−0.510 (−0.797)	0.339 (0.361)
M4	0.139 (0.135)	0.618 (0.596)	0.242 (0.269)	0.633 (0.596)	−0.191 (−0.209)	0.557 (0.613)	0.494 (0.461)	−0.809 (−0.805)	0.315 (0.344)

[a] $\Delta q = q(S_1) - q(S_0)$. Values obtained in vacuum are given in parentheses.

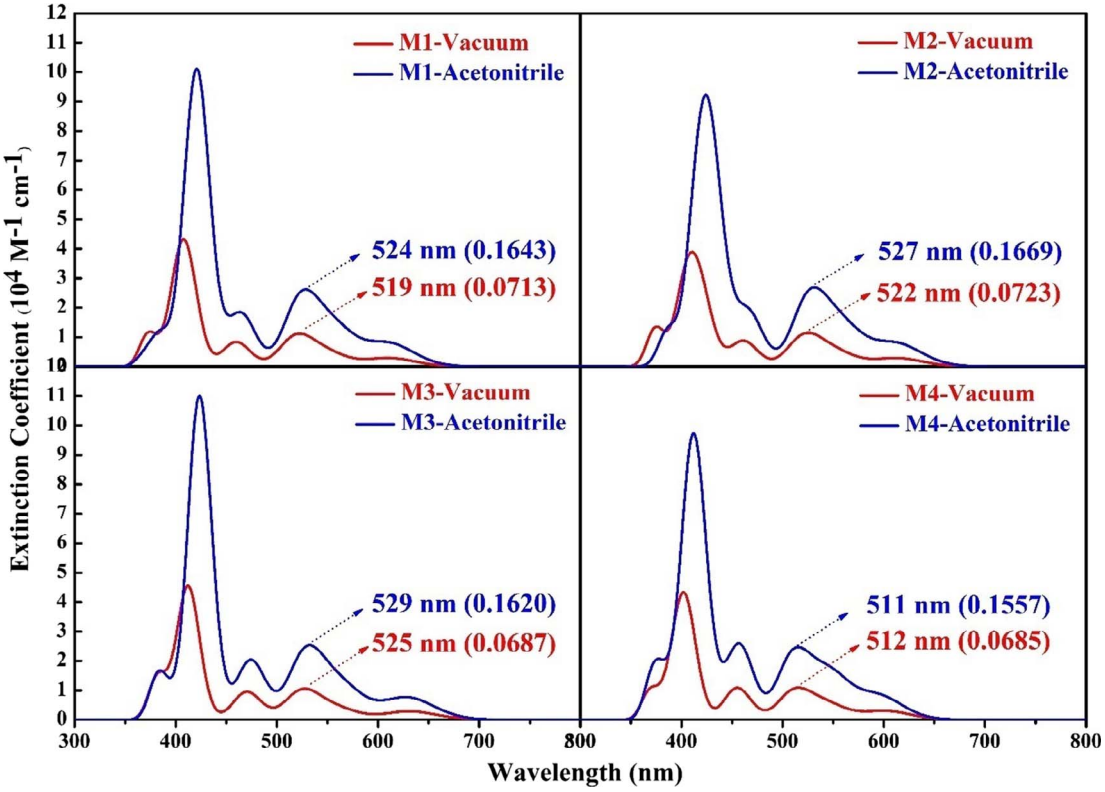

Fig. 5. Comparison of the optical absorption spectra of the four sensitizers in acetonitrile (blue) and in a vacuum (red). (For interpretation of the references to color in this figure legend, the reader is referred to the web version of this article.)

Table 3
Calculated absorptions corresponding to the major peaks (λ > 500 nm) and the oscillator strengths of the four sensitizers in solvent. The wavelengths, bandgaps, and oscillator strengths given in parentheses were obtained in a vacuum.

Dye	λ (nm)	Bandgap $E_{0\text{-}0}$ (eV)[a]	Excitation state	Oscillator strength (*f*)	LHE[b]	Predominant transition
M1	611 (612)	1.70 (1.66)	$S_0 \rightarrow S_2$	0.0522 (0.0197)	0.113 (0.044)	H-2 → LUMO (94%)
	559 (552)		$S_0 \rightarrow S_4$	0.0788 (0.0267)	0.166 (0.060)	H-1 → LUMO (77%)
	524 (519)		$S_0 \rightarrow S_5$	0.1643 (0.0713)	0.315 (0.151)	H-1 → L + 1 (97%)
M2	613 (614)	1.64 (1.59)	$S_0 \rightarrow S_2$	0.0515 (0.0193)	0.112 (0.043)	H-2 → LUMO (94%)
	561 (554)		$S_0 \rightarrow S_4$	0.0818 (0.0284)	0.172 (0.063)	H-1 → LUMO (77%)
	527 (522)		$S_0 \rightarrow S_5$	0.1669 (0.0723)	0.319 (0.153)	H-1 → L + 1 (96%)
M3	629 (631)	1.66 (1.62)	$S_0 \rightarrow S_2$	0.0513 (0.0195)	0.111 (0.044)	H-2 → LUMO (93%)
	566 (561)		$S_0 \rightarrow S_4$	0.0702 (0.0229)	0.149 (0.051)	H-1 → LUMO (73%)
	529 (525)		$S_0 \rightarrow S_5$	0.1620 (0.0687)	0.311 (0.146)	H-1 → L + 1 (97%)
M4	596 (602)	1.84 (1.74)	$S_0 \rightarrow S_2$	0.0533 (0.0202)	0.115 (0.045)	H-2 → LUMO (95%)
	548 (5 4 5)		$S_0 \rightarrow S_4$	0.0999 (0.0322)	0.205 (0.071)	H-1 → LUMO (79%)
	511 (5 1 2)		$S_0 \rightarrow S_5$	0.1557 (0.0685)	0.301 (0.146)	H-1 → L + 1 (97%)

[a] $S_0 \rightarrow S_1$ excitation energy.
[b] Light harvesting efficiency.

in shape with the presence of the solvent; instead, a small bathochromic shift of *ca*. 5 nm for dyes **M1** to **M3** and a negligible1 nm hypsochromic shift for dye **M4** were observed in the solvent. The change in the absorption position is insignificant but the absorbance (oscillator strength) increased substantially, i.e., a hyperchromic shift occurred with the inclusion of the solvent. Table 3 lists the simulated photophysical properties of the dyes obtained by employing TDDFT formalism in the solvent and vacuum. We reported only three absorptions (λ > 500 nm) with significant oscillator strengths for each dye. The three peaks arose from the singlet excitation to S_2, S_4, and S_5 states from the S_0 state. The intense absorption in the low energy region (λ_{max}) for **M1** to **M4** in the solvent are 524, 527, 529, and 511 nm, respectively, and the corresponding absorption values in a vacuum were 519, 522, 525, and 512. The transition responsible for λ_{max} for each dye is of HOMO − 1 → LUMO + 1 character. From the molecular orbital composition (*vide supra*), it is clear that the photoexcitation is due predominantly to the charge transfer phenomenon from the metal to ligand. Therefore, the simulated optical spectra of the dyes do not undergo a substantial shift but have stronger absorption strength in the solvent.

The light harvesting efficiency (LHE) of the sensitizer affects the short-circuit current density (J_{SC}), and hence, the overall power conversion efficiency (η). The calculated LHEs with the oscillator strength at each absorption wavelength are listed in the same table. Interestingly, the LHEs obtained in the solvent were 2–3 times higher than those obtained in the vacuum.

3.2. Dyes adsorbed on $(TiO_2)_{38}$ cluster

The sensitizers adsorbed on TiO_2 surface was examined because the

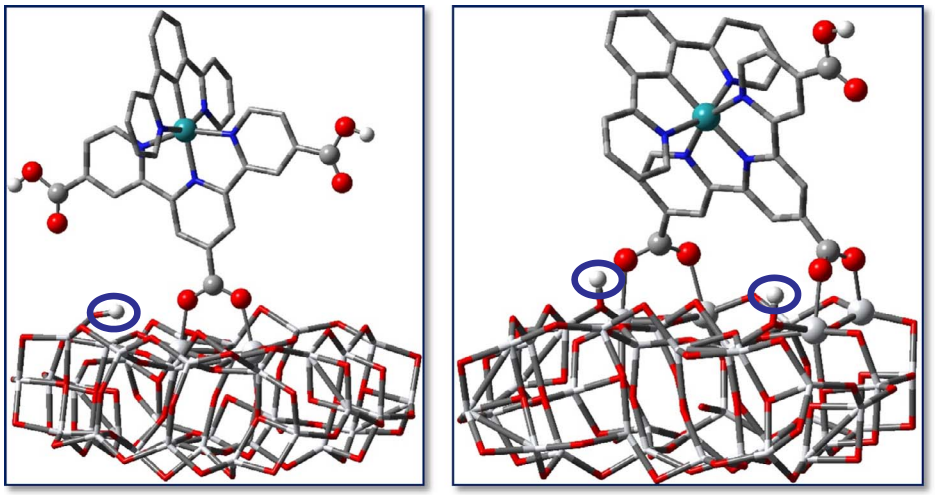

Fig. 6. Optimized structures of **M1** dye tethered to the $(TiO_2)_{38}$ cluster with one (left) and two (right) COOH anchored. The hydrogens attached to the carbons are omitted here for clarity. The encircled hydrogen atoms on TiO_2 are dissociated from the anchoring carboxylic group(s).

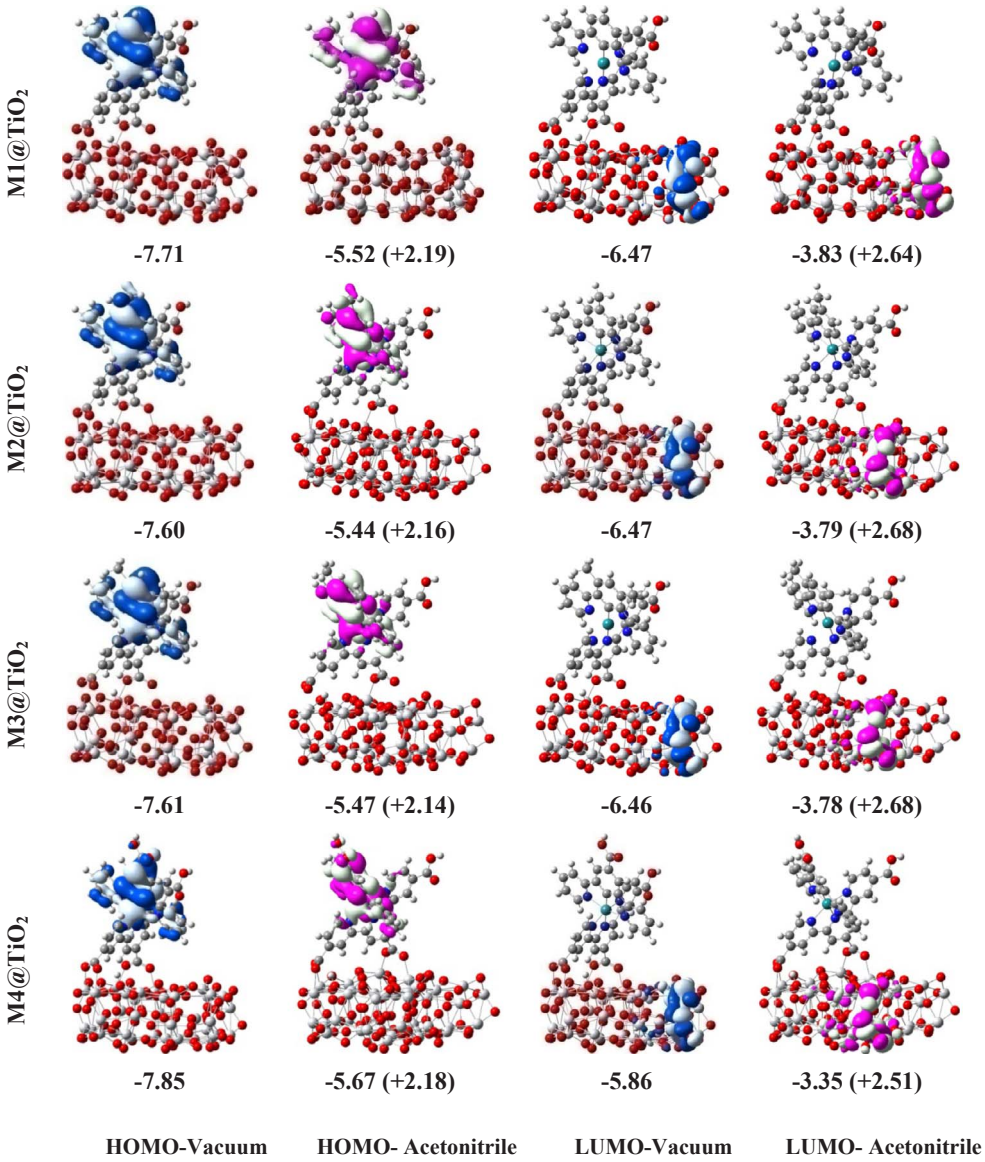

Fig. 7. Comparison of the frontier molecular orbitals and their energies (eV) of the dye@TiO_2 assemblies with two COOH adsorption in acetonitrile vs. in vacuum. The magnitude of destabilization due to the solvent is shown in parenthesis.

binding nature and the electronic coupling of an excited state dye with the TiO_2 conduction band can strongly affect the efficiency of a DSSC device. The adsorption of an inorganic complex $[Fe(CN)_6]^{4-}$ on TiO_2 has been studied by first principles computational investigation (De Angelis et al., 2004). Persson and Lundqvist (2005) performed DFT studies of the ruthenium polypyridyl complex (**N3**) attached to a TiO_2 cluster. A

Table 4
Simulated absorption maxima (λ_{max}), oscillator strengths, and wavefunction coefficients of dye@TiO_2 assemblies with 1-COOH and 2-COOH anchoring in the solvent. The wavelengths and oscillator strengths obtained in vacuum are given in parentheses.

Dye	Dye adsorbed with	λ_{max} (nm)	Excitation state	Oscillator strength (*f*)	Predominant transition
M1	1-COOH	523 (518)	$S_0 \rightarrow S_{22}$	0.0837 (0.0584)	H-1 → L + 24(68%)
	2-COOH	547 (543)	$S_0 \rightarrow S_{16}$	0.1343 (0.1012)	H-1 → L + 15 (17%)
M2	1-COOH	524 (520)	$S_0 \rightarrow S_{18}$	0.0765 (0.0316)	H-1 → L + 24(75%)
	2-COOH	548 (545)	$S_0 \rightarrow S_{17}$	0.1346 (0.1023)	H-1 → L + 21 (17%)
M3	1-COOH	527 (524)	$S_0 \rightarrow S_{24}$	0.0799 (0.0539)	H-2 → L + 24 (54%)
	2-COOH	550 (548)	$S_0 \rightarrow S_{17}$	0.1250 (0.0964)	H-2 → L + 21 (13%)
M4	1-COOH	512 (512)	$S_0 \rightarrow S_{17}$	0.0828 (0.0576)	H-1 → L + 20 (51%)
	2-COOH	531 (534)	$S_0 \rightarrow S_9$	0.1203 (0.0911)	H-1 → L + 13 (21%)

dye binds to TiO_2 with its anchoring COOH group in a monodentate or bidentate form. The bidentate binding can be either chelating or bridging. The binding modes and nature of the dye onto the TiO_2 surface can be distinguished experimentally by empirical rules based on vibrational frequency analysis.

Bidentate bridging is a stable adsorption mode over the other possible chemisorption modes (Srinivas et al., 2009). In the bidentate bridging mode, the adsorption can be either dissociative or undissociative. In dissociative adsorption, the carboxylic hydrogen is transferred to a nearby oxygen atom of TiO_2 surface and the two carboxylic oxygen atoms form bonds with two titanium atoms. Given that the dissociative bidentate bridging mode is more favorable than the undissociative bidentate bridging (De Angelis et al., 2007a,b) mode, all the calculations were carried out in dissociative bidentate bridging mode. The dyes investigated have three carboxylic groups on their TPY ligands and the adsorption studies were carried out with two possibilities, as depicted in Fig. 6. The adsorption of the dye (**M1**) with anchoring of two carboxylic groups is more stable than that with one carboxylic group by 14.20 kcal/mol.

3.2.1. Interfacial electronic structure and frontier molecular orbitals of dye@TiO_2assemblies

The optimized geometries of the dye@TiO_2 assemblies were used to calculate the energies of FMOs and the electron density distribution in the gas phase (vacuum) and in the solvent. Fig. 7 shows the Kohn-Sham eigenvalues and the electron density distribution in FMOs of the assemblies (with 2-COOH anchoring). The electron density is localized mainly around the TPY-C ligand of the sensitizer in the HOMO and is shifted to TiO_2 in the LUMO of the assemblies. No significant change in the electron density distribution in the presence of the solvent was observed. The HOMO energy levels of all the assemblies obtained in a vacuum are lower than −7.60 eV and the lowest value was obtained for M4@TiO_2 (−7.85 eV). In the solvent, the HOMO energies of the assemblies were upshifted by more than 2.10 eV but they are still close and below the redox potential of I^-/I_3^-. In particular, the HOMO energy levels of the assemblies do not vary significantly from those of the isolated dyes, as the electron densities in both cases are localized predominantly around the sensitizer. In addition, the LUMO energy levels of the assemblies in the solvent were upshifted by more than 2.50 eV. The destabilization observed for the LUMOs is more than that found for the HOMOs. The order of the FMO energy levels of the assemblies in the solvent is consistent with the trend observed in a vacuum. The HLG values of the dye@TiO_2 assemblies follow the same trend observed for the isolated dyes in a vacuum and in solvent. Fig. S3 of the Supplementary Information presents the electron density distribution and Kohn-Sham eigenvalues of the FMOs of dye@TiO_2 assemblies with 1-COOH anchoring. Figs. S4 (vacuum) and S5 (acetonitrile) of the Supplementary Information compare the energies of FMOs of the TiO_2 cluster with those of dye@TiO_2 assemblies.

3.2.2. Optical properties of the dye@TiO_2assemblies in solvent

Using the optimized geometries of the dye@TiO_2 assemblies in the TDDFT calculations, their UV-visible absorption spectra were obtained both in the vacuum and solvent. Table 4 lists the absorption maxima along with their oscillator strengths (*f*) and wavefunction coefficients of four assemblies with 1-COOH and 2-COOH anchoring. From the calculated optical absorption data, the spectra covered the 400–700 nm region and showed an intense absorption at approximately 550 nm. The absorption spectrum of the M3@TiO_2assembly had longer absorption (red-shifted) than that of the other assemblies. A considerable bathochromic shift (*ca.* 20 nm) in absorption was achieved for dye@TiO_2 assemblies (with anchoring of two COOH groups) relative to those of the isolated sensitizers. The electron density in the reported virtual molecular orbitals (Table 4), involved in the photo excitations, is localized on the dye and on TiO_2. The TDDFT simulations showed an extra absorption peak around 640 nm, which indicates direct electron transfer from the dye (excited state) to the anode (De Angelis, 2010). The solvent yielded a modest and negligible bathochromic shift (< 5 nm) in the absorption with an enhanced intensity, except for M4@TiO_2. From the calculated oscillator strengths, the assemblies showed a substantial hyperchromic shift, as observed for isolated ruthenium sensitizers.

4. Conclusions

A detailed first-principles investigation was carried out to gain deeper insights into the geometry, electronic structure, and optical properties of four thiocyanate free cyclometalated ruthenium dyes either isolated or adsorbed on a TiO_2 surface. The effects of solvation were examined by simulating the cases with and without an acetonitrile solvent. The FMO energy levels were upshifted uniformly by *ca.* 2.2 eV from those of vacuum but the HLG values remained relatively unchanged. Upon solvation, the LUMOs of the dyes are in energetically close proximity to bind to TiO_2 and the HOMOs of the dyes are in line with the redox potential of I^-/I_3^- to facilitate the dye regeneration process. With solvation, the position of absorption peaks did not change considerably but a more than twofold hyperchromic shift have been observed. For the dyes adsorbed on a TiO_2 cluster, the solvent induced an upshift of more than 2.10 eV for the HOMO and more than 2.50 eV for the LUMO energies of the assemblies. The non-uniform upshifts in HOMO and LUMO eigenvalues of the assemblies yielded a different HLG in the solvent from vacuum. The dye@TiO_2assemblies showed absorptions redshifted by almost 20 nm from those of isolated sensitizers. The shift in the absorption wavelength of the assemblies due to the solvent was in significant but their absorption intensity was substantial.

Acknowledgements

This study was supported by the National Research Foundation of Korea (NRF) grant funded by the Korea government (NRF-2015R1A2A2A01004208, NRF-2014R1A4A1001690, and NRF-2016-

H1D3A1936765).

Conflict of interest

The authors declare no conflict of interest.

Appendix A. Supplementary material

Supplementary data associated with this article can be found, in the online version, at http://dx.doi.org/10.1016/j.solener.2017.10.058.

References

Ardo, S., Meyer, G.J., 2009. Photo driven heterogeneous charge transfer with transition-metal compounds anchored to TiO_2 semiconductor surfaces. Chem. Soc. Rev. 38, 115–164.

Becke, A.D., 1993. Density-functional thermochemistry. III. The role of exact exchange. J. Chem. Phys. 98, 5648–5652.

Bessho, T., Yoneda, E., Yum, J.-H., Guglielmi, M., Tavernelli, I., Imai, H., Rothlisberger, U., Nazeeruddin, M.K., Grätzel, M., 2009. New paradigm in molecular engineering of sensitizers for solar cell applications. J. Am. Chem. Soc. 131, 5930–5934.

Blöchl, P.E., 1994. Projector augmented-wave method. Phys. Rev. B 50, 17953–17979.

Byrne, A., English, N.J., Schwingenschlögl, U., Coker, D.F., 2016. Dispersion and solvation effects on the structure and dynamics of N719 adsorbed to anatase titania (101) surfaces in room-temperature ionic liquids: an ab initio molecular simulation study. J. Phys. Chem. C 120, 21–30.

De Angelis, F., Tilocca, A., Selloni, A., 2004. Time-dependent DFT study of $[Fe(CN)_6]^{4-}$ sensitization of TiO_2 nanoparticles. J. Am. Chem. Soc. 126, 15024–15025.

De Angelis, F., Fantacci, S., Selloni, A., Grätzel, M., Nazeeruddin, M.K., 2007a. Influence of the sensitizer adsorption mode on the open-circuit potential of dye-sensitized solar cells. Nano Lett. 7, 3189–3195.

De Angelis, F., Fantacci, S., Selloni, A., Nazeeruddin, M.K., Grätzel, M., 2007b. Time-dependent density functional theory investigations on the excited states of Ru(II)-dye-sensitized TiO_2 nanoparticles: the role of sensitizer protonation. J. Am. Chem. Soc. 129, 14156–14157.

De Angelis, F., 2010. Direct vs. indirect injection mechanisms in perylene dye-sensitized solar cells: a DFT/TDDFT investigation. Chem. Phys. Lett. 493, 323–327.

Di Valentin, C., Pacchioni, G., Selloni, A., 2006. Electronic structure of defect states in hydroxylated and reduced rutile TiO_2(110) surfaces. Phys. Rev. Lett. 97, 166803.

Fantacci, S., De Angelis, F., Sgamellotti, A., Re, N., 2004. A TDDFT study of the ruthenium (II) polyazaaromatic complex $[Ru(dppz)(phen)_2]^{2+}$ in solution. Chem. Phys. Lett. 396, 43–48.

Frisch, M.J., Trucks, G.W., Schlegel, H.B., Scuseria, G.E., Robb, M.A., Cheeseman, J.R., Scalmani, G., Barone, V., Mennucci, B., Petersson, G.A., Nakatsuji, H., Caricato, M., Li, X., Hratchian, H.P., Izmaylov, A.F., Bloino, J., Zheng, G., Sonnenberg, J.L., Hada, M., Ehara, M., Toyota, K., Fukuda, R., Hasegawa, J., Ishida, M., Nakajima, T., Honda, Y., Kitao, O., Nakai, H., Vreven, T., Montgomery, J.A., Jr., Peralta, J.E., Ogliaro, F., Bearpark, M., Heyd, J.J., Brothers, E., Kudin, K.N., Staroverov, V.N., Kobayashi, R., Normand, J., Raghavachari, K., Rendell, A., Burant, J.C., Iyengar, S.S., Tomasi, J., Cossi, M., Rega, N., Millam, J.M., Klene, M., Knox, J.E., Cross, J.B., Bakken, V., Adamo, C., Jaramillo, J., Gomperts, R., Stratmann, R.E., Yazyev, O., Austin, A.J., Cammi, R., Pomelli, C., Ochterski, J.W., Martin, R.L., Morokuma, K., Zakrzewski, V. G., Voth, G.A., Salvador, P., Dannenberg, J.J., Dapprich, S., Daniels, A.D., Farkas, Ö., Foresman, J.B., Ortiz, J.V., Cioslowski, J., Fox, D.J. Gaussian 09, Revision D.01. Gaussian Inc, Wallingford CT, 2013.

Hay, P.J., Wadt, W.R., 1985. Ab initio effective core potentials for molecular calculations. Potentials for the transition metal atoms Sc to Hg. J. Chem. Phys. 82, 270–283.

Karelson, M.M., Zerner, M.C., 1992. Theoretical treatment of solvent effects on electronic spectroscopy. J. Phys. Chem. 96, 6949–6957.

Kresse, G., Hafner, J., 1993. *Ab initio* molecular dynamics for liquid metals. Phys. Rev. B 47, 558–561.

Kresse, G., Furthmüller, J., 1996. Efficiency of ab-initio total energy calculations for metals and semiconductors using a plane-wave basis set. Comput. Mater. Sci. 6, 15–50.

Kresse, G., Joubert, D., 1999. From ultrasoft pseudopotentials to the projector augmented-wave method. Phys. Rev. B 59, 1758–1775.

Lee, C., Yang, W., Parr, R.G., 1988. Development of the Colle-Salvetti correlation-energy formula into a functional of the electron density. Phys. Rev. B 37, 785–789.

Liu, S.-H., Fu, H., Cheng, Y.-M., Wu, K.-L., Ho, S.-T., Chi, Y., Chou, P.-T., 2012. Theoretical study of N749 dyes anchoring on the $(TiO_2)_{28}$ surface in DSSCs and their electronic absorption properties. J. Phys. Chem. C 116, 16338–16345.

Lundqvist, M.J., Nilsing, M., Persson, P., Lunell, S., 2006. DFT study of bare and dye-sensitized TiO_2 clusters and nanocrystals. Int. J. Quantum Chem. 106, 3214–3234.

Makov, G., Payne, M.C., 1995. Periodic boundary conditions in *ab initio* calculations. Phys. Rev. B 51, 4014–4022.

Mathew, S., Yella, A., Gao, P., Humphry-Baker, R., CurchodBasile, F.E., Ashari-Astani, N., Tavernelli, I., Rothlisberger, U., NazeeruddinMd, K., Grätzel, M., 2014. Dye-sensitized solar cells with 13% efficiency achieved through the molecular engineering of porphyrin sensitizers. Nat. Chem. 6, 242–247.

Nazeeruddin, M.K., Péchy, P., Renouard, T., Zakeeruddin, S.M., Humphry-Baker, R., Comte, P., Liska, P., Cevey, L., Costa, E., Shklover, V., Spiccia, L., Deacon, G.B., Bignozzi, C.A., Grätzel, M., 2001. Engineering of efficient panchromatic sensitizers for nanocrystalline TiO_2-based solar cells. J. Am. Chem. Soc. 123, 1613–1624.

Neugebauer, J., Scheffler, M., 1992. Adsorbate-substrate and adsorbate-adsorbate interactions of Na and K adlayers on Al(111). Phys. Rev. B 46, 16067–16080.

O'Regan, B., Grätzel, M., 1991. A low-cost, high-efficiency solar cell based on dye-sensitized colloidal TiO_2 films. Nature 353, 737–740.

Pastore, M., Etienne, T., De Angelis, F., 2016. Structural and electronic properties of dye-sensitized TiO_2 for solar cell applications: from single molecules to self-assembled monolayers. J. Mater. Chem. C 4, 4346–4373.

Perdew, J.P., Burke, K., Ernzerhof, M., 1996. Generalized gradient approximation made simple. Phys. Rev. Lett. 77, 3865–3868.

Persson, P., Lundqvist, M.J., 2005. Calculated structural and electronic interactions of the ruthenium dye N3 with a titanium dioxide nanocrystal. J. Phys. Chem. B 109, 11918–11924.

Singh, S.P., Sharma, G.D., 2014. Near infrared organic semiconducting materials for bulk hetero junction and dye-sensitized solar cells. Chem. Rec. 14, 419–481.

Srinivas, K., Yesudas, K., Bhanuprakash, K., Rao, V.J., Giribabu, L., 2009. A combined experimental and computational investigation of anthracene based sensitizers for DSSC: comparison of cyanoacrylic and malonic acid electron withdrawing groups binding onto the TiO_2 anatase (101) surface. J. Phys. Chem. C 113, 20117–20126.

Szafran, M., Karelson, M.M., Katritzky, A.R., Koput, J., Zerner, M.C., 1993. Reconsideration of solvent effects calculated by semiempirical quantum chemical methods. J. Comput. Chem. 14, 371–377.

Tapia, O., Goscinski, O., 1975. Self-consistent reaction field theory of solvent effects. Mol. Phys. 29, 1653–1661.

Tuyet Nguyen, P., Rand Andersen, A., Morten Skou, E., Lund, T., 2010. Dye stability and performances of dye-sensitized solar cells with different nitrogen additives at elevated temperatures—Can sterically hindered pyridines prevent dye degradation? Sol. Energy Mater. Sol. Cells 94, 1582–1590.

Wadman, S.H., Kroon, J.M., Bakker, K., Lutz, M., Spek, A.L., van Klink, G.P.M., van Koten, G., 2007. Cyclometalated ruthenium complexes for sensitizing nanocrystalline TiO_2 solar cells. Chem. Commun. 1907–1909.

Wong, M.W., Wiberg, K.B., Frisch, M.J., 1992. Solvent effects. 2. Medium effect on the structure, energy, charge density, and vibrational frequencies of sulfamic acid. J. Am. Chem. Soc. 114, 523–529.

Xu, Y., Chen, W.-K., Cao, M.-J., Liu, S.-H., Li, J.-Q., Philippopoulos, A.I., Falaras, P., 2006. A TD-DFT study on the electronic spectrum of $Ru(II)L_2$ [L = bis(5′-methyl-2,2′-bipyridine-6-carboxylato)] in the gas phase and DMF solution. Chem. Phys. 330, 204–211.